Formation and manipulation of ferrofluid droplets at a microfluidic *T*-junction

2010 J. Micromech. Microeng. 20 045004

(http://iopscience.iop.org/0960-1317/20/4/045004)

J. Micromech. Microeng. **20** (2010) 045004 (10pp) doi:10.1088/0960-1317/20/4/045004

Formation and manipulation of ferrofluid droplets at a microfluidic *T*-junction

Say-Hwa Tan[1,2], Nam-Trung Nguyen[1,3], Levent Yobas[2] and Tae Goo Kang[2]

[1] School of Mechanical and Aerospace Engineering, Nanyang Technological University, 50 Nanyang Avenue, Singapore 639798
[2] Institute of Microelectronics, Science Park II, Singapore 117685

E-mail: mntnguyen@ntu.edu.sg

Received 15 October 2009, in final form 8 December 2009
Published 5 March 2010
Online at stacks.iop.org/JMM/20/045004

Abstract

This paper reports the formation and manipulation of ferrofluid droplets at a microfluidic *T*-junction in the presence of a permanent magnetic field. A small circular permanent magnet with a diameter of 3 mm is used to control the size of the ferrofluid droplets within a microfluidic device. In the absence of a magnetic field, the size of the ferrofluid droplets decreases linearly with the increase of the flow rate of the continuous phase. In the presence of a magnetic field, the size of the droplets depends on the magnetic field strength, magnetic field gradient and the magnetization of the ferrofluid. The magnetic field strength is adjusted in our experiment by the location of the magnet. The induced attractive magnetic force affects the droplet formation process leading to the change in the size of the formed droplets. Experimental observation also shows that the relative change in the size of the droplet depends on the flow rate of the continuous phase. Furthermore, the paper compares the evolving shape of the ferrofluid droplet during the formation process with and without the magnetic field.

(Some figures in this article are in colour only in the electronic version)

1. Introduction

Droplet-based microfluidics involves the generation and manipulation of discrete droplets in microscale [1]. In contrast to continuous-flow microfluidics, droplet-based microfluidics allows the control of individual droplets. The compartmentalization of liquid within a droplet is useful for many applications [2], where each droplet can be individually transported, mixed and analysed [3, 4]. In addition, the high surface area to volume ratio and the shorter characteristic time of heat and mass transfer in microscale allows faster reaction which is favoured by many biological and chemical applications [5, 6]. Therefore, the controllable generation and manipulation of droplets are important research topics [7].

The generation and manipulation of droplets are achieved by either passive or active means. Passive methods generate and manipulate droplets with different channel configurations such as a *T*-junction [8–14] and flow focusing [15–21]. However, these fixed channel configurations only allow the manipulation of droplets by hydrodynamic means. Active methods handle droplets with externally induced means such as thermal effects [22–28], pressure [29, 30], electrowetting [31, 32], dielectrophoresis [33] and thermo capillarity [34].

Recently, magnetism has been combined with microfluidics in an amazing variety of ways [35]. For instance, magnetic nanoparticles attached to biomolecules have been widely applied in biochemical separation [36], immunoassay [37] and targeted drug delivery [38]. Ferrofluid is a class of nanofluids that contains magnetic nanoparticles. Ferrofluid was used as droplets or plugs in polymerase chain reactor (PCR) [39–41], micropumps [42–44], electromagnetic pipette [45], drug carriers [46], valve [47], optical filter [48], mixer [49] and detection of surface defects [50]. In the above-mentioned applications, the size of the ferrofluid droplet is an important parameter because its volume and the corresponding magnetization determine the magnetic force needed for the actuation. To our best knowledge, only a very few studies have been reported on the manipulation of the droplet size in a confined microfluidic channel.

[3] To whom correspondence should be addressed.

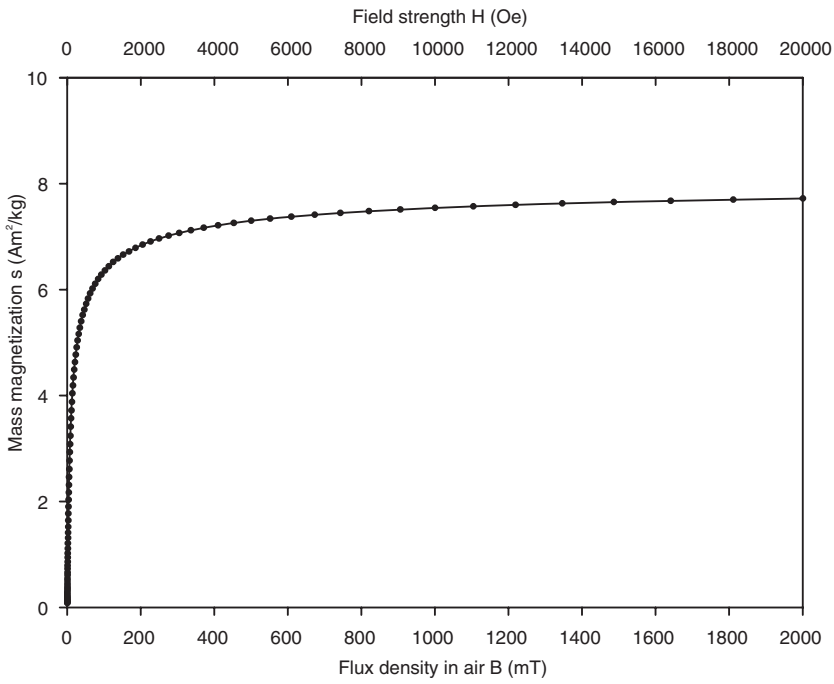

Figure 1. Magnetization curves of the ferrofluid used in our experiments (EMG807, Ferrotech, at 300 K). The data were obtained from the manufacturer's data sheet. The field strength is depicted as the corresponding flux density in air for easy comparison with later measured field data. The magnetization M is calculated from the depicted mass magnetization s as $M = s\rho$, where ρ is the density of the ferrofluid. At the lower field strength, a small change in the magnetic field results in a substantial change in the magnetization of the ferrofluid. The saturation magnetization of the ferrofluid is reached if the magnetic flux in air is about 500 mT.

This paper presents a chip-based method to control the size of the ferrofluid droplets generated at a microfluidic T-junction. The influence of capillary number, flow rates and magnetic field strengths on the formation process is experimentally investigated and discussed. The use of an external permanent magnet allows controlling the size of the formed ferrofluid droplets even if the flow rates of the continuous phase and the dispersed phase are kept constant.

2. Manipulation concept

As mentioned above, ferrofluid is a special category of smart materials, in particular magnetically controllable nanofluids. These fluids are colloids of magnetic nanoparticles which consist of mainly Fe_3O_4 magnetites with a diameter of about 10 nm [51, 52]. The nanoparticles are dispersed in a carrier fluid such as water or oil. The surface of each particle is often covered with a surfactant to prevent the agglomeration of particles due to the van der Waals force [53]. Brownian motion prevents the particles from settling under gravity and keeps them randomly dispersed throughout the carrier fluid in the absence of a magnetic field [54, 55]. The small size of each particle and its superparamagnetic property allows the control of the magnetic property of the ferrofluid with negligible hysteresis [56]. In the absence of a magnetic field, the magnetic nanoparticles are randomly distributed and thus the ferrofluid has no net magnetization. If a water-based ferrofluid and oil work as the dispersed and continuous phases at a microfluidic T-junction, uniform ferrofluid droplets can be generated. The size of each ferrofluid droplet is then determined by the geometry, the flow rates and the capillary number, i.e. the balance between viscous force and the capillary force.

However, in the presence of an external magnetic field, the single-domain colloidal magnetite particles will automatically align themselves along the magnetic field and become magnetized [57]. The magnetization of the fluid interacts with the external magnetic field to produce an attractive body force in the direction of the highest magnetic field. This attractive force on the ferrofluid per unit volume is given by

$$F_{\mathrm{m}} = \mu_0 M \nabla H, \tag{1}$$

where μ_0 is the magnetic permeability of free space, M is the magnetization and ∇H is the gradient of the external magnetic field strength. Figure 1 illustrates the magnetization curves for a commercially available ferrofluid (EMG 807, Ferrotech), which is used later in our experiments. Figure 1 shows that in contrast to the zero-field case [58], a small magnetic field will have a substantial effect in the magnetization of the ferrofluid as long as the magnetic field is below the saturation point. This change in magnetization reduces significantly when the ferrofluid reaches saturation. For the ferrofluid used in our later experiments, the saturation magnetization is approximately 7.3 A m^2 kg^{-1} when the magnetic field is about 500 mT (flux density in air).

Equation (1) indicates that the attractive magnetic force is proportional to the magnetization and the gradient of the external magnetic field. The field magnitude and its gradient can be adjusted by the distance between the ferrofluid and a permanent magnet. Since the magnetization is proportional to

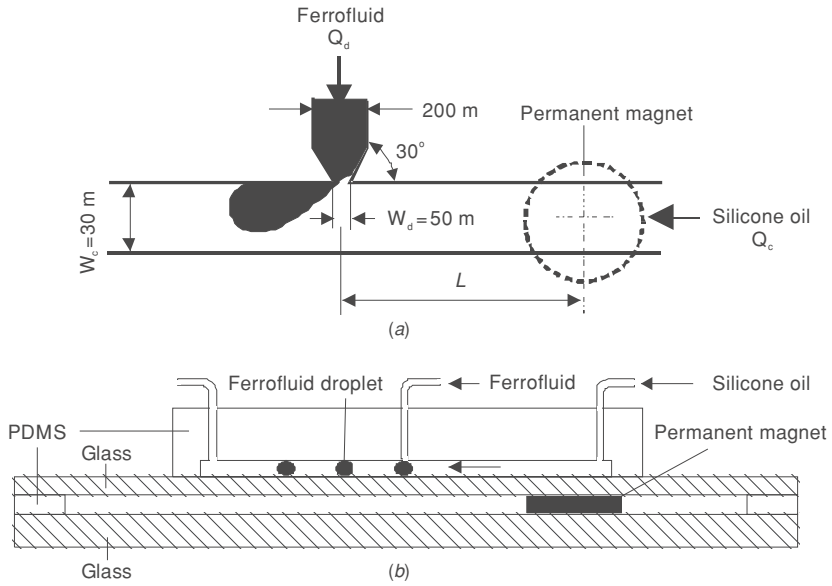

Figure 2. Schematics of the experimental setup for the formation of ferrofluid droplets at a microfluidic *T*-junction (not to scale): (*a*) the microfluidic network; (*b*) the setup with the permanent magnet. The PDMS layer separating the glass and magnet in (*b*) acts as a support for the microfluidic chip. It has the same thickness of approximately 2 mm as the magnet.

the magnitude of the field, both magnitude and gradient can be used to manipulate and control the size of the ferrofluid droplets formed at a microfluidic *T*-junction. The magnitude and direction of the magnetic field and the corresponding magnetic force can be easily adjusted by changing the location of the magnet and the separation distance between the ferrofluid and the magnet.

3. Materials and methods

The test devices were fabricated in polydimethylsiloxane (PDMS) using the soft lithography technique [59–61]. The design was printed on a transparency film with a resolution of 8000 dpi. The transparency mask was subsequently used for defining the negative SU-8 mould of the microchannels. Sylgard 184 silicone elastomer was purchased from Dow Corning. PDMS was mixed with a weight ratio of 10:1 and poured onto the SU-8 master mould. Thereafter, PDMS was vacuumed for 2 h to remove the gas bubbles. After the degassing process, PDMS was heated at 80 °C for 2 h. The PDMS part was then peeled off from the master mould and fluidic access holes of 0.75 mm were created using a manual puncher (Harris Uni-Core, World Precision Instruments, Inc., FL, USA). The PDMS with the microchannels was subsequently bonded to a flat piece of glass of 0.13 mm thickness using oxygen plasma treatment (790 Series, Plasma-Therm, Inc., FL, USA). A 24 h room temperature curing process ensures the hydrophobic recovery of the PDMS microchannel. The channel has a height of 100 μm. The inlet widths of the microchannels for the continuous phase and the dispersed phase are 300 μm and 50 μm, respectively. The schematic device and experimental setup are shown in figure 2.

An epi-fluorescent inverted microscope was used to observe the droplet formation process. A CCD camera (Edmund Optics, EO-0413C) was used for recording images. The fluids were delivered to the device by precision syringe pumps (KD Scientific Inc., USA). A small circular neodymium iron boron (NdFeB) magnet of 3 mm diameter and 2 mm thickness generates the external magnetic field needed for the experiments.

In our experiments, ferrofluid (EMG 807, Ferrotech) works as the dispersed phase. The carrier liquid of the ferrofluid is water. At 27 °C, the kinematic viscosity and density of the ferrofluid are $\nu = 2$ cSt s and $\rho = 1100$ kg m^{-3}, respectively. The volume concentration of this ferrofluid is 1.8%. The initial susceptibility of this ferrofluid is $\chi = 0.39$. The magnetic nanoparticle has an average diameter of about 10 nm. As the particle size is small, the magnetoviscous effect is negligible [62–64]. Silicone oil (Sigma-Aldrich) works in the droplet formation experiments as the continuous phase. The kinematic viscosity and density of silicone oil are $\nu = 100$ cSt s and $\rho = 960$ kg m^{-3}, respectively. The interfacial tension between the ferrofluid and silicone oil was measured using a commercial tensiometer (Lauda's TVT-2) and is approximately $\sigma = 21.1$ mN m^{-1}.

4. Results and discussions

4.1. Ferrofluid droplet formation in a microchannel

The first experiment was designed to investigate the formation mechanism and the effect of the continuous flow on the ferrofluid droplets at a microfluidic *T*-junction. The flow rate of the dispersed phase Q_d was fixed at 10 μl h^{-1}, while the flow rate of the continuous phase varies from $Q_c = 50$ to 150 μl h^{-1}. The flow rates were chosen to cover the transition from the squeezing to the dripping regime [65–67]. The droplet diameter was measured using a customized

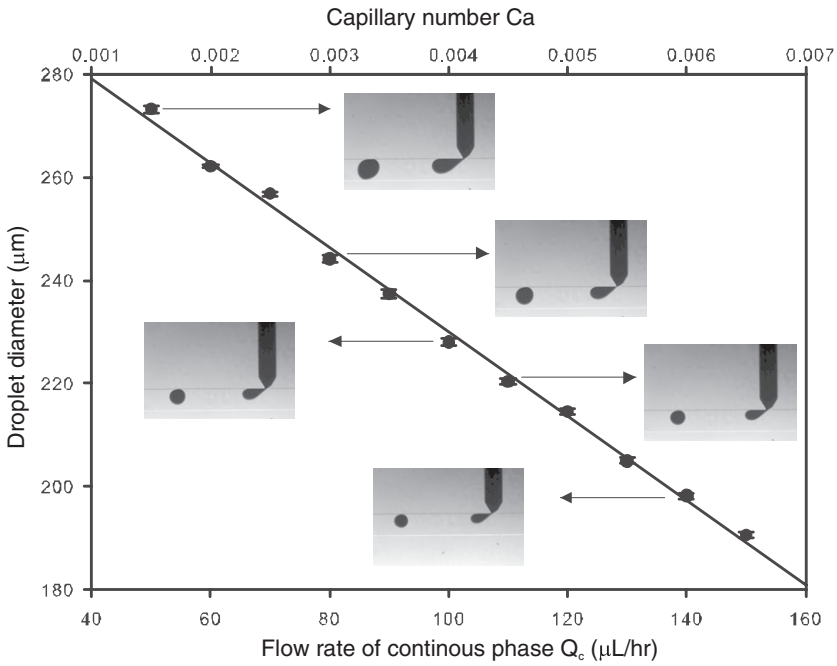

Figure 3. Droplet diameter as a function of the flow rate of the continuous phase Q_c as well as of the capillary number Ca. The dispersed phase is fixed at $Q_d = 10\ \mu l\ h^{-1}$.

MATLAB program. The relationship between the droplet diameter and the flow rate as well as the capillary number is shown in figure 3. The capillary number defined in terms of the continuous phase is often used to distinguish the droplet formation regimes:

$$\mathrm{Ca} = \frac{U_c \mu_c}{\lambda} = \frac{Q_c \mu_c}{\sigma w_c h}, \tag{2}$$

where μ_c is the dynamic viscosity, Q_c is the continuous phase flow rate, σ is the interfacial tension between the fluids, $w_c = 300\ \mu m$ is the width of the channel and $h = 100\ \mu m$ is the channel height.

The image sequences were processed using another customized MATLAB program. The MATLAB program reads each image frame and crops it to the region of interest. Subsequently, the greyscale image was converted into a binary image which clearly shows the ferrofluid as a black area. An edge detection algorithm was subsequently applied to visualize the line representing the interface between the evolving droplet and the continuous phase. Overlapping the interface images results in the time-evolving image of the ferrofluid droplet during the formation process. This image serves as a good visualization tool for the droplet formation process. Figure 4 shows the typical evolution of a ferrofluid droplet at the *T*-junction at two different continuous flow rates $Q_c = 50\ \mu l\ h^{-1}$ and $Q_c = 100\ \mu l\ h^{-1}$.

The results show that as the continuous flow rate Q_c increases, the diameter of the droplets decreases. A high continuous flow rate increases the viscous shear stress. The magnitude of the viscous shear stress can be estimated by the product of $\mu_c G$, where μ_c is the dynamic viscosity of the continuous phase. The characteristic shear rate G is proportional to the flow rate Q_c. The magnitude of the squeezing pressure is determined by the gap between the emerging interface and the opposite wall of the microchannel. Increasing the flow rate of the continuous phase decreases the squeezing pressure. Figure 4 shows that the radius of curvature of the interface becomes smaller and the gap between it and the channel wall grows as the flow rate of the continuous phase increases. In addition, increasing the flow rate of the continuous phase decreases the duration of the formation process significantly. Visual observation confirms that the formation mechanism depends on both the viscous shear rate and the squeezing pressure. Droplets formed in this transition regime are affected by both the capillary number and flow rate ratio [64].

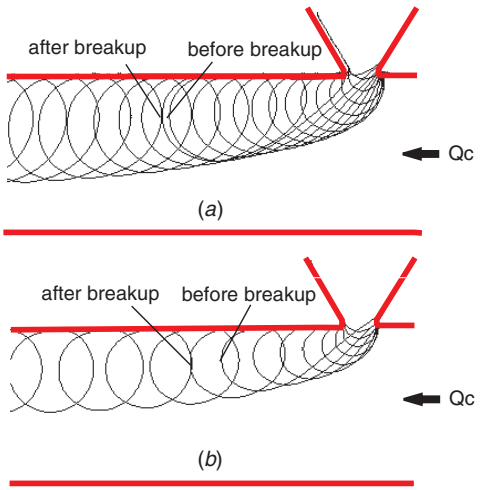

Figure 4. Measured formation process of the ferrofluid in the absence of an external magnetic field ($Q_d = 10\ \mu l\ h^{-1}$, delay time between each frame 0.08 s): (*a*) $Q_c = 50\ \mu l\ h^{-1}$; (*b*) $Q_c = 100\ \mu l\ h^{-1}$.

Figure 3 shows a linear relationship between the droplet diameters and the flow rate of the continuous phase as well as the capillary numbers. The range of capillary number from approximately 0.002 to 0.006 corresponds to the transition between the squeezing regime and the dripping regime. In this transition regime, the dynamics of droplet breakup is dominated by both viscous shear stress and squeezing pressure [65–67]. The results of formation of ferrofluid droplets in the absence of an magnetic field therefore agree with the previous experimental observation and hypotheses about the viscous stress and squeezing pressure caused by the continuous phase.

4.2. Ferrofluid droplet formation in a magnetic field

The second experiment used a permanent magnet to adjust the gradient and the magnitude of the magnetic field at the *T*-junction. To vary the magnitude of the magnetic force on the ferrofluid, the magnet was placed at distances ranging from 2.3 mm to 3.8 mm away from the centre of the microchannel for ferrofluid. To change the direction of the attractive magnetic force, the magnet was placed either upstream or downstream relative to the dispersed phase channel. The distance was measured using a customized MATLAB program. Figure 2(*b*) shows the schematic sketch of the experimental setup.

Fixed flow rates of $Q_d = 10\ \mu l\,h^{-1}$ and $Q_c = 100\ \mu l\,h^{-1}$ were used in this experiment. To avoid interferences between each experiment, the magnet was removed and placed again into the new position. A settling time of 15 min before capturing and recording the images was allowed for each new position of the magnet. Figure 5 compares the formation process of a ferrofluid droplet without the magnet, with a magnet placed 2.3 mm upstream of the *T*-junction and with a magnet 2.3 mm downstream of the *T*-junction. The results show that under the same flow rates of $Q_d = 10\ \mu l\ h^{-1}$ and $Q_c = 100\ \mu l\ h^{-1}$, the curvature of the interface changes when the magnet is placed upstream or downstream of the *T*-junction. When the magnet is placed upstream, the curvature becomes steeper as shown in figure 5(*b*). However, when the magnet is placed downstream with the same distance apart, the interface is more curved as shown in figure 5(*c*). As the radius of curvature affects the size of formed droplets [68], this observation affirms that magnetic force can be used to control the size of the droplets formed at a microfluidic *T*-junction.

We used a calibration measurement to determine the magnetic flux as a function of the distance to the centre of the permanent magnet. Figure 6 shows the measured magnetic flux density and the corresponding field gradient as a function of the distance. The magnetic flux density of the permanent magnet was measured using a commercial gaussmeter with an accuracy of 1% (Hirst, GM05, UK). A micropositioner (M4508-DM, Parker Hannifin) was used to align and adjust the distance between the magnet and the probe. The same sheet of glass of thickness 0.13 mm was placed between the magnet and the probe to emulate the situation in the droplet formation experiment. Figure 6 shows that the magnetic flux density and magnetic field gradient clearly decrease with increasing distance. The measured data depicted in figure 6 are fitted

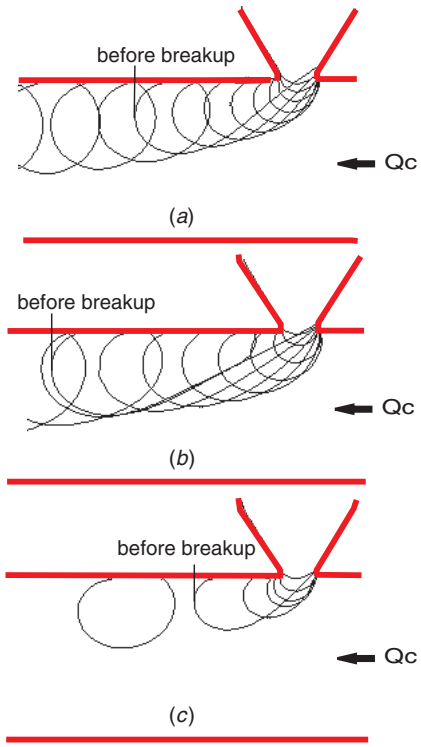

Figure 5. Measured formation process of ferrofluid droplets at $Q_d = 10\ \mu l\ h^{-1}$ and $Q_c = 100\ \mu l\ h^{-1}$ (delay time between each frame 0.08 s): (*a*) without permanent magnet; (*b*) permanent magnet upstream at a distance of 2.3 mm ($B = 27.2$ mT); and (*c*) permanent magnet downstream at a distance of 2.3 mm ($B = 27.2$ mT).

with a second-order polynomial function to determine the flux density as a function of the distance to the centre of the magnet:

$$B(x) = 1.25x^2 - 16.8x + 59.2, \tag{3}$$

where the units of x and B are mm and mT, respectively. This relationship shows that the further away the magnet, the smaller are the field magnitude and the field gradient.

Figure 7 shows the droplet size as a function of the magnetic flux density derived from the distance between the permanent magnet and the *T*-junction. If the magnet is placed upstream of the *T*-junction, the size of the ferrofluid droplets is larger than those without an external magnet. However, as the magnet is shifted further upstream, the size of the droplets decreases and approaches the size of droplets formed without the magnet. The difference becomes insignificant when the magnet is placed at a distance beyond 4 mm or when the flux density is less than 12 mT. In contrast, when the magnet is placed downstream of the *T*-junction, the size of the droplets is smaller than those without an external magnet. Again, the difference in the droplets size becomes insignificant when the flux density is less than 12 mT. As mentioned above, the magnitude of the attractive magnetic force is proportional to both the magnetization of the ferrofluid and the magnetic field gradient. At a position closer to the centre of the permanent magnet, the larger magnetization caused by the large field magnitude together with the higher gradient results in a large attractive force [69, 70]. However, if the separation distance increases, the magnetic force also decreases as both

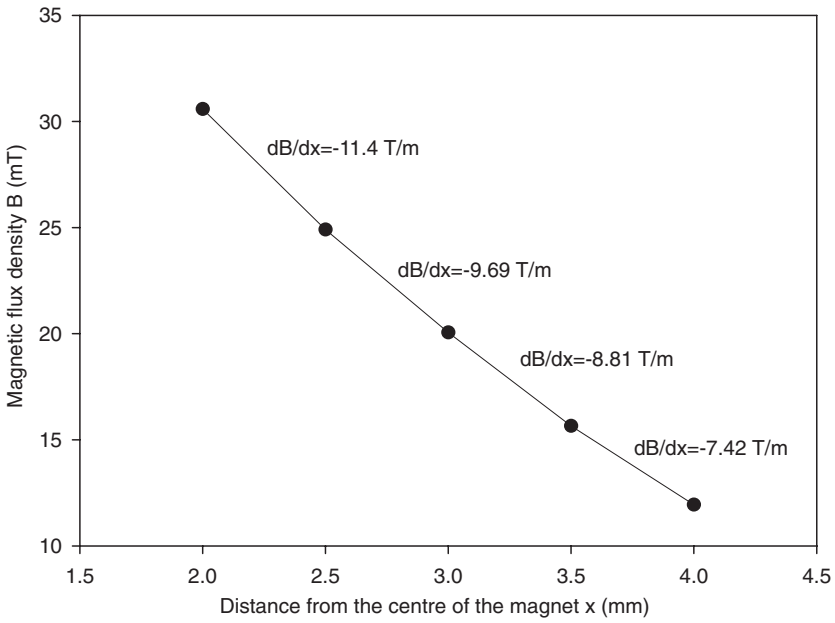

Figure 6. Measured magnetic flux density of the permanent magnet as a function of distance.

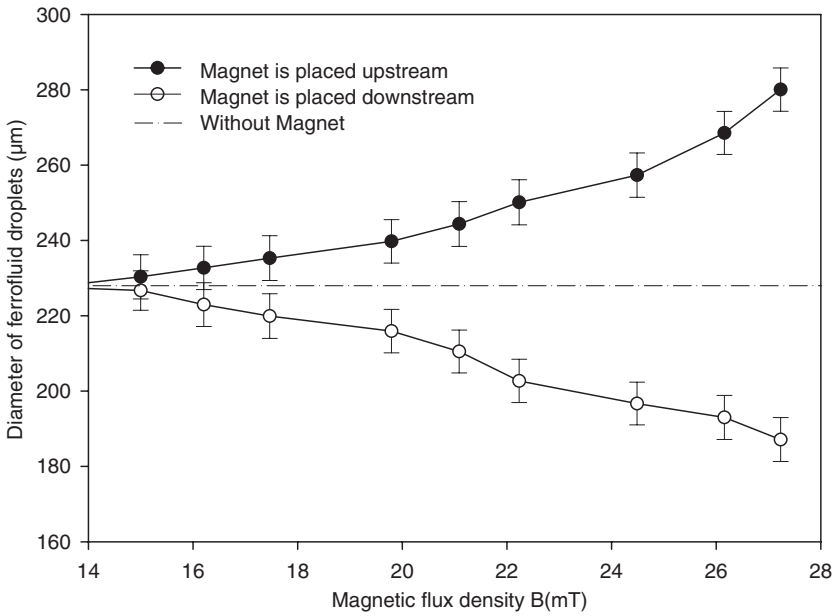

Figure 7. Diameter of the ferrofluid droplet as a function of the magnetic flux density for both upstream and downstream cases. The dashed line represents the diameter of the formed droplets in the absence of the magnet. In all three cases, the flow rate of the dispersed phase is fixed at $Q_d = 10\ \mu l\ h^{-1}$ and the continuous phase is fixed at $Q_c = 100\ \mu l\ h^{-1}$.

the magnetization of the ferrofluid and the gradient of the magnetic field decrease.

4.3. Effect of field strength and location of the magnet

The location of the permanent magnet relative to the *T*-junction also plays an important role in influencing the size of the formed droplets. If the permanent magnet is placed at the upstream position, the magnetic force pulls the emerging droplet back and delays the breakup process. This pulling force allows more dispersed ferrofluid to emerge, holding it longer at the *T*-junction. Hence, a larger droplet is formed after the breakup. The breakup moment was captured in figure 5(*b*) by the sudden change in the displacement of the advancing interface of the droplet. The effect of the holding force can be clearly observed here. In the absence of the magnetic field, the droplet breaks up before the receding interface becomes flat or its radius of curvature goes to infinity, figure 5(*a*). With a magnet upstream, the droplet cannot break up even when the receding interface becomes flat. In this case, the interface force reaches its minimum value, but the increasing viscous drag force and the increasing squeezing pressure need to balance with increasing magnetic force. Figure 8 shows

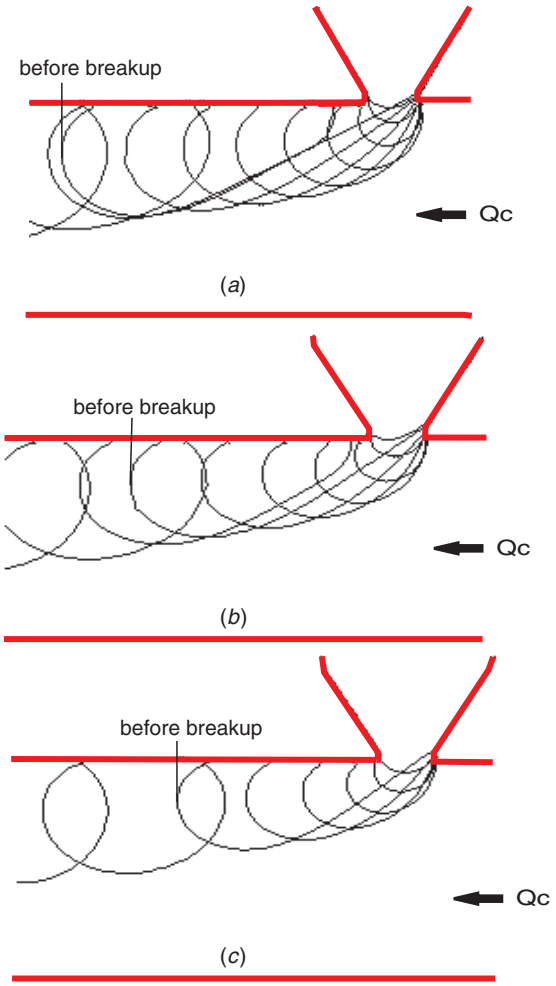

Figure 8. Measured formation process of ferrofluid at $Q_d = 10\ \mu l\ h^{-1}$ and $Q_c = 100\ \mu l\ h^{-1}$ (delay time between each frame 0.08 s). The magnet is placed at different upstream positions: (*a*) at a distance of 2.3 mm ($B = 27.2$ mT); (*b*) at a distance of 2.8 mm ($B = 22.0$ mT); and (*c*) at a distance of 3.8 mm ($B = 13.4$ mT).

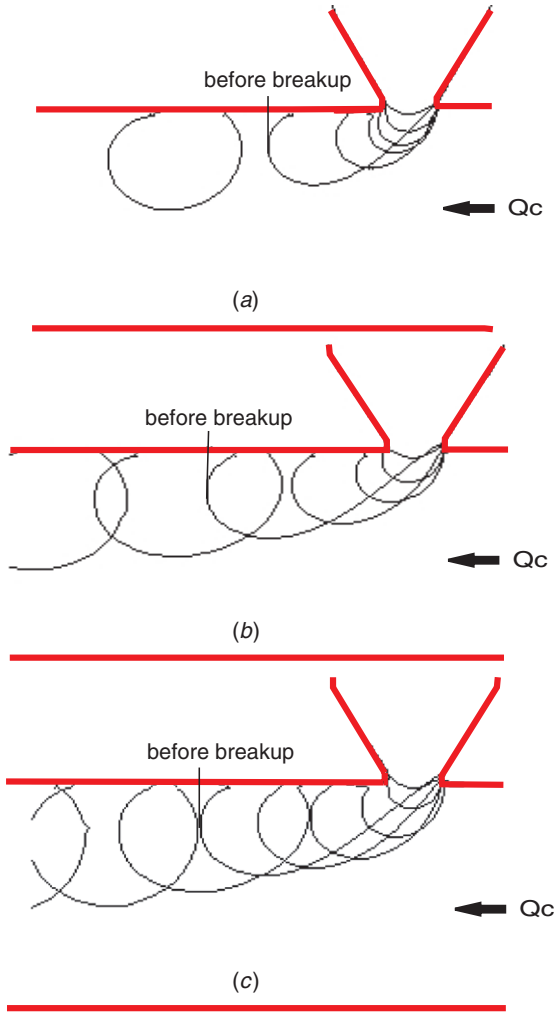

Figure 9. Measured formation process of ferrofluid at $Q_d = 10\ \mu l\ h^{-1}$ and $Q_c = 100\ \mu l\ h^{-1}$ (delay time between each frame 0.08 s). The magnet is placed at different downstream positions: (*a*) at a distance of 2.3 mm ($B = 27.2$ mT); (*b*) at a distance of 2.8 mm ($B = 22.0$ mT); and (*c*) at a distance of 3.8 mm ($B = 13.4$ mT).

the droplet formation process, when the magnet is placed at different upstream locations.

In contrast, if the magnet is placed at the downstream position, the magnetic force pulls the emerging ferrofluid droplet forward, figure 5(*c*). In this case, the pulling magnetic force accelerates the breakup process. Breakup occurs at a radius of curvature of the receding interface smaller than that of the case without the magnet as shown in figure 5(*a*). A fast breakup process results in smaller droplets as less ferrofluid is allowed to join the droplet prior to breakup. Figure 9 shows the droplet formation process with the magnet placed at different downstream locations.

4.4. Effect of different continuous phase flow rates in the presence of a magnetic field

In a droplet formation process without any external field, the effect of continuous flow on the size of the formed droplet is significant. In most cases, the droplet diameter decreases with the increase in the flow rate of the continuous phase and vice versa. With the presence of a magnetic field, the effect of the continuous phase could be different. In order to investigate the role of the continuous phase under the influence of a magnetic field, the same experiment was repeated using another set of flow rates of $Q_d = 10\ \mu l\ h^{-1}$ and $Q_c = 150\ \mu l\ h^{-1}$. Figure 10 shows the relative change in the droplet diameter versus the flux density. We found that a lower flow rate of the continuous phase results in a larger change in the droplet diameter. The curve of $Q_c = 100\ \mu l\ h^{-1}$ has a much steeper slope. These phenomena can be explained by the nature of the magnetic force as a volume force. The magnetic force acting on the ferrofluid is proportional to its volume emerging into the continuous phase. At a higher flow rate of $Q_c = 150\ \mu l\ h^{-1}$, the volume of the ferrofluid in the continuous phase is smaller; hence, a magnetic force has a smaller magnitude as compared to the case of $Q_c = 100\ \mu l\ h^{-1}$. This fact results in a relatively smaller change in the droplets size.

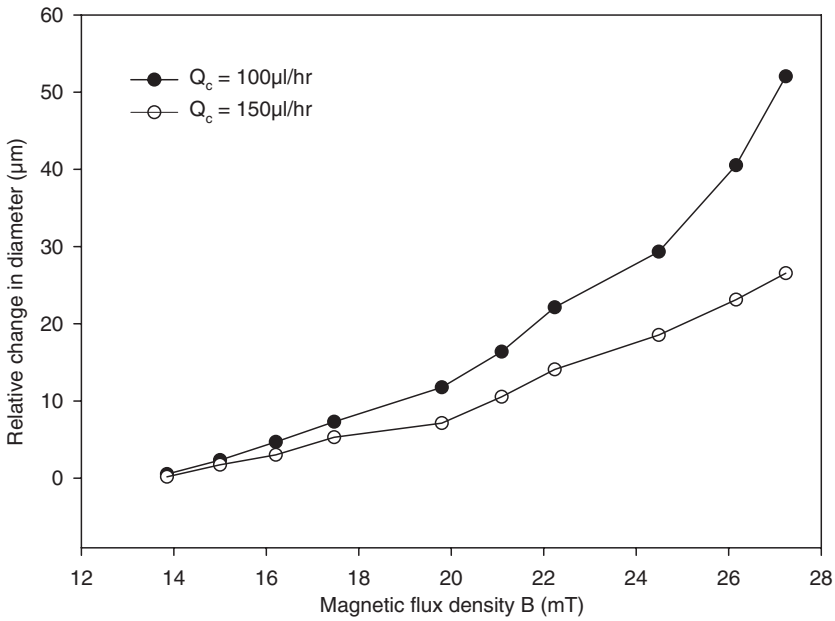

Figure 10. Influences of flow rates of the continuous phase on the change in the droplet diameter. The dispersed phase is fixed at a flow rate of $Q_d = 10\ \mu l\,h^{-1}$.

5. Conclusions

We have developed a new route for controlling the size of a droplet by using an external permanent magnet. In the absence of a magnetic field, the diameter of the formed droplets varies linearly with the flow rate of the continuous phase. A higher flow rate of the continuous phase results in droplets with a smaller diameter. Experimental observations suggest that both the viscous shear stress and the 'squeezing' pressure are the dominant mechanisms in the droplet breakup process. The corresponding capillary numbers verify this observation as the droplet formation process lies within the transition region between the squeezing and the dripping regimes. In the presence of a magnetic field, the diameter of the droplets can be controlled by the magnetic field gradient, the magnetization of the ferrofluid and the relative position of the magnet. When the magnet is placed upstream of the *T*-junction, the magnetic force pulls the emerging droplet back and delays the breakup process. The delay allows more dispersed ferrofluid to flow into the continuous phase, thus forming bigger droplets. The distance between the magnet and ferrofluid determines the magnitude of the magnetic force acting on the emerging ferrofluid. A larger separation distance results in a weaker magnetic force, leading to the formation of relatively smaller droplets. When the magnet is placed downstream, the magnetic force accelerates the breakup process. The magnetic force pulls the ferrofluid and causes the formation of smaller droplets. The pulling force and the droplet diameter can also be adjusted by the distance between the magnet and the *T*-junction. Formation processes with and without the external magnet were compared. The magnetic forces exerted on the emerging fluid change the radius of curvature at the interface during the droplet formation process. A steeper curvature is observed during the droplet formation process when the magnet is placed upstream. However, the net effect of the magnetic force is a complex problem in which the evolving shape of the droplet also plays an important role. Only a complex three-dimensional numerical model with coupled fields could give more insights into the observed phenomena reported in this paper. Furthermore, we discussed the effect of different continuous phase flow rates in the presence of a magnetic field. A higher continuous phase flow causes a smaller difference in the droplet diameter because the magnitude of the magnetic force is proportional to the volume of the droplet. A relatively smaller flow rate of the continuous phase forms bigger droplets due to the presence of a larger volume.

Acknowledgments

The authors gratefully acknowledge the support from the Agency of Science, Technology and Research (A*STAR), Singapore (grant number SERC 052 101 0108 'Droplet-based micro/nanofluidics').

References

[1] Teh S Y, Lin R, Hung L H and Lee A P 2008 Droplet microfluidics *Lab Chip* **8** 198–220
[2] Christopher G F and Anna S L 2007 Microfluidic methods for generating continuous droplet streams *J. Phys. D: Appl. Phys* **40** R319–36
[3] Fair R B 2007 Digital microfluidics: is a true lab-on-a-chip possible? *Microfluid Nanofluid* **3** 245–81
[4] Link D R, Grasland-Mongrain E, Duri A, Sarrazin F, Cheng Z D, Cristobal G, Marquez M and Weitz D A 2006 Electric control of droplets in microfluidic devices *Angew. Chem. Int. Edn* **45** 2556–60
[5] Reyes D R, Iossifidis D, Auroux P A and Manz A 2002 Micro total analysis systems: 1. Introduction, theory, and technology *Anal. Chem.* **74** 2623–36

[6] Vilkner T, Janasek D and Manz A 2004 Micro total analysis systems recent developments *Anal. Chem.* **76** 3373–85

[7] Zhang K, Liang Q L, Ma S, Mu X, Hu P, Wang Y M and Luo G A 2009 On-chip manipulation of continuous picoliter-volume superparamagnetic droplets using a magnetic force *Lab Chip* **9** 2992–9

[8] Thorsen T, Roberts R W, Arnold F H and Quake S R 2001 Dynamic pattern formation in a vesicle-generating microfluidic device *Phys. Rev. Lett.* **86** 4163–6

[9] Nisisako T, Torii T and Higuchi T 2002 Droplet formation in a microchannel network *Lab Chip* **2** 24–6

[10] Xu J H, Luo G S, Li S W and Chen G G 2006 Shear force induced monodisperse droplet formation in a microfluidic device by controlling wetting properties *Lab Chip* **6** 131–6

[11] Garstecki P, Fuerstman M J, Stone H A and Whitesides G M 2006 Formation of droplets and bubbles in a microfluidic T-junction—scaling and mechanism of break-up *Lab Chip* **6** 437–46

[12] van der Graaf S, Steegmans M L J, van der Sman R G M, Schröen C G P H and Boom R M 2005 Droplet formation in a T-shaped microchannel junction: a model system for membrane emulsification *Colloids Surf.* A **266** 106–16

[13] Gupta A, Murshed S M S and Kumara R 2009 Droplet formation and stability of flows in a microfluidic T-junction *Appl. Phys. Lett.* **94** 164107

[14] Husny J and Cooper-White J J 2006 The effect of elasticity on drop creation in T-shaped microchannels *J. Non-Newtonian Fluid Mech.* **137** 121–36

[15] Anna S L, Bontoux N and Stone H S 2003 Formation of dispersions using 'flow focusing' in microchannels *Appl. Phys. Lett.* **82** 364–6

[16] Anna S L and Mayer H C 2006 Microscale tipstreaming in a microfluidic flow focusing device *Phys. Fluids* **18** 121512

[17] Ong W L, Hua J, Zhang B, Teo T Y, Zhuo J L, Nguyen N T, Ranganathan N and Yobas L 2007 Experimental and computational analysis of droplet formation in a high-performance flow-focusing geometry *Sensors Actuators* A **138** 203–12

[18] Tan Y C, Cristini V and Lee A P 2006 Monodispersed microfluidic droplet generation by shear focusing microfluidic device *Sensors Actuators* B **114** 350–6

[19] Wu N, Zhu Y, Leech P W, Sexton B A, Brown S and Easton C 2008 Effects of surfactants on the formation of microdroplets in the flow focusing microfluidic device *Proc. SPIE* **6799** 67990C

[20] Ward T, Faivre M, Abkarian M and Stone H A 2005 Microfluidic flow focusing: drop size and scaling in pressure versus flow-rate-driven pumping *Electrophoresis* **26** 3716–24

[21] Xu Q Y and Nakajima M 2004 The generation of highly monodisperse droplets through the breakup of hydrodynamically focused microthread in a microfluidic device *Appl. Phys. Lett.* **85** 3726–8

[22] Farahi R H, Passian A, Ferrell T L and Thundat T 2004 Microfluidic manipulation via Marangoni forces *Appl. Phys. Lett.* **85** 4237–9

[23] Nguyen N T, Ting T H, Yap Y F, Wong T N, Chai J C K, Ong W L, Zhou J L, Tan S H and Yobas L 2007 Thermally mediated droplet formation in microchannels *Appl. Phys. Lett.* **91** 084102

[24] Murshed S M S, Tan S H and Nguyen N T 2008 Temperature dependence of interfacial properties and viscosity of nanofluids for droplet-based microfluidics *J. Phys. D: Appl. Phys.* **41** 085502

[25] Murshed S M S, Tan S H, Nguyen N T, Wong T N and Yobas L 2009 Microdroplet formation of water and nanofluids in heat-induced microfluidic T-junction *Microfluid Nanofluid* **6** 253–9

[26] Tan S H, Murshed S M S, Nguyen N T, Wong T N and Yobas L 2008 Thermally controlled droplet formation in flow focusing geometry—formation regimes and effects of nanoparticle suspension *J. Phys. D: Appl. Phys.* **41** 165501

[27] Yap Y F, Tan S H, Nguyen N T, Wong T N and Yobas L 2009 Thermally mediated control of liquid microdroplets at a bifurcation *J. Phys. D: Appl. Phys.* **42** 065503

[28] Ting T H, Yap Y F, Nguyen N T, Wong T N and Chai J C K 2006 Thermally mediated breakup of drops in microchannels *Appl. Phys. Lett.* **89** 234101

[29] Sassa F, Fukuda J and Suzuki H 2008 Microprocessing of liquid plugs for bio/chemical analyses *Anal. Chem.* **80** 6206–13

[30] Lee C Y, Lin Y H and Lee G B 2009 A droplet-based microfluidic system capable of droplet formation and manipulation *Microfluid Nanofluid* **6** 599–610

[31] Srinivasan V, Pamula V K and Fair R B 2004 An integrated digital microfluidic lab-on-a-chip for clinical diagnostics on human physiological fluids *Lab Chip* **4** 310–5

[32] Abdelagwad M, Freire S L S, Yang H and Wheeler A R 2008 All-terrain droplet actuation *Lab Chip* **8** 672–7

[33] Velev O D, Prevo B G and Bhatt K H 2003 On-chip manipulation of free droplets. *Nature* **426** 515–6

[34] Baroud C N, Delville J P, Gallaire F and Wunenburger R 2007 Thermocapillary valve for droplet production and sorting *Phys. Rev.* E **75** 046302

[35] Pamme N 2006 Magnetism and microfluidics *Lab Chip* **6** 24–38

[36] Doyle P S, Bibette J, Bancaud A and Viovy J L 2002 Self-assembled magnetic matrices for DNA separation chips *Science* **295** 2237

[37] Nam J M, Thaxton C S and Mirkin C A 2003 Nanoparticle-based bio-bar codes for the ultrasensitive detection of proteins *Science* **301** 1884–6

[38] Yu M K, Jeong Y Y, Park J, Park S, Kim J W, Min J J, Kim K and Jon S 2008 Drug-loaded superparamagnetic iron oxide nanoparticles for combined cancer imaging and therapy *in vivo Angew. Chem. Int. Edn* **47** 5362–5

[39] Sun Y, Kwok Y C, Lee P F P and Nguyen N T 2009 Rapid amplification of genetically modified organisms using a circular ferrofluid-driven PCR microchip *Anal. Bioanal. Chem.* **394** 1505–8

[40] Sun Y, Nguyen N T and Kwok Y C 2007 High-throughput polymerase chain reaction in parallel circular loops using magnetic actuation *Anal. Chem.* **80** 6127–30

[41] Sun Y, Kwok Y C and Nguyen N T 2007 A circular ferrofluid driven microchip for rapid polymerase chain reaction *Lab Chip* **7** 1012–7

[42] Hatch A, Kamholz A E, Holman G, Yager P and Böhringer K F A 2001 A ferrofluidic magnetic micropump *J. Microelectromech. Syst.* **10** 215–21

[43] Nguyen N T and Chai M F 2009 A stepper micropump for ferrofluid driven microfluidic systems *Micro Nanosystems* **1** 17–21

[44] Yamahata C, Chastellain M, Parashar V K, Petri A, Hofmann H and Gijs M A M 2005 Plastic micropump with ferrofluidic actuation *J. Microelectromech. Syst.* **14** 132–7

[45] Greivell N E and Hannaford B 1997 The design of a ferrofluid magnetic pipette *IEEE Trans. Biomed. Eng.* **44** 129–35

[46] Ruuge E K and Rusetski A N 1993 Magnetic fluids as drug carriers: targeted transport of drugs by a magnetic field *J. Magn. Magn. Mater.* **122** 335–9

[47] Hartshorne H, Backhouse C J and Lee W E 2004 Ferrofluid-based microchip pump and valve *Sensors Actuators* B **99** 592–600

[48] Philip J, Jaykumar T, Kalyanasundaram P and Raj B 2003 A tunable optical filter *Meas. Sci. Technol.* **14** 1289–94

[49] Oh D W, Jin J S, Choi J H, Kim H Y and Lee J S 2007 A microfluidic chaotic mixer using ferrofluid *J. Micromech. Microeng.* **17** 2077–83
[50] Philip J, Rao C B, Raj B and Jayakumar T 1999 An optical technique for the detection of surface defects in ferromagnetic samples *Meas. Sci. Technol.* **10** N71–5
[51] Rosenzweig R E 1985 *Ferrohydrodynamics* (Cambridge: Cambridge University Press) 344 pp
[52] Berkowsky B M, Medvedev V F and Krakov M S 1993 *Magnetic Fluids Engineering Applications* (New York: Oxford University Press)
[53] Berger P, Adelman N B, Beckman K J, Campbell D J, Ellis A B and Lisensky G C 1999 *J. Chem. Educ.* **76** 943–8
[54] Zahn M 2001 Magnetic fluid and nanoparticle applications to nanotechnology *J. Nanoparticle Res.* **3** 73–8
[55] Ytreberg F M and McKay S R 2000 Calculated properties of field-induced aggregates in ferrofluids *Phys. Rev.* E **61** 4107–10
[56] Miranda J A and Oliveira R M 2004 Adhesion phenomena in ferrofluids *Phys. Rev.* E **70** 036311
[57] Oliveira R M and Miranda J A 2008 Ferrofluid patterns in a radial magnetic field: linear stability, nonlinear dynamics and exact solutions *Phys. Rev.* E **77** 016304
[58] Borglin S E, Moridis G J and Oldenburg C 2000 Experimental studies of the flow of ferrofluid in porous media *Transp. Porous Media* **41** 61–80
[59] Ng J M K, Gitlin I, Stroock A D and Whitesides G M 2002 Components for integrated poly(dimethylsiloxane) microfluidic systems *Electrophoresis* **23** 3461–73
[60] McDonald J C, Duffy D C, Anderson J R, Chiu D T, Wu H, Schueller O J A and Whitesides G M 2000 Fabrication of microfluidic systems in poly(dimethylsiloxane) *Electrophoresis* **21** 27–40
[61] Sia S K and Whitesides G M 2003 Microfluidic devices fabricated in poly(dimethylsiloxane) for biological studies *Electrophoresis* **24** 3563–76
[62] Odenbach S 2003 Ferrofluids—magnetically controlled suspensions *Colloids Surf.* A **217** 171–8
[63] Felderhof B U 2000 Magnetoviscosity and relaxation in ferrofluids *Phys. Rev.* E **62** 3848–54
[64] Odenbach S 2000 Magnetoviscous and viscoelastic effects in ferrofluids *Int. J. Mod. Phys.* B **14** 1615–31
[65] Xu J H, Li S W, Tan J and Luo G S 2008 Correlations of droplet formation in T-junction microfluidic devices: from squeezing to dripping *Microfluid Nanofluid* **5** 711–7
[66] De Menech M, Garstecki P, Jousse F and Stone H A 2008 Transition from squeezing to dripping in a microfluidic T-shaped junction *J. Fluid Mech.* **595** 141–61
[67] Christopher G F, Noharuddin N N, Taylor J A and Anna S L 2008 Experimental observations of the squeezing-to-dripping transition in T-shaped microfluidic junctions *Phys. Rev.* E **78** 036317
[68] van der Graaf S, Nisisako T, Schron C G P H, van der Sman R G M and Boom R M 2006 Lattice Boltzmann simulations of droplet formation in a T-shaped microchannel *Langmuir* **22** 4144–52
[69] Afkhami S, Renardy Y, Renardy M, Riffle J S and Pierre T S 2008 Field-induced motion of ferrofluid droplets through immiscible viscous media *J. Fluid Mech.* **610** 363–80
[70] Banerjee S, Fasnacht M, Garoff S and Widom M 1999 Elongation of confined ferrofluid droplets under applied fields *Phys. Rev.* E **60** 4272–9